PNAS NEXUS

Repeated glucose oscillations in high cell–density cultures influence stress–related functions of *Escherichia coli*

Jonas Bafna-Rührer [ID][a], Yashomangalam D. Bhutada [ID][a], Jean V. Orth [ID][a], Süleyman Øzmerih [ID][a], Lei Yang[a], Daniel Zielinski [ID][b] and Suresh Sudarsan [ID][a,*]

[a]The Novo Nordisk Foundation Center for Biosustainability, Technical University of Denmark, 2800 Kongens Lyngby, Denmark
[b]Department of Bioengineering, University of California, San Diego, CA 92093-0412, USA
*To whom correspondence should be addressed: Email: sursud@biosustain.dtu.dk
Edited By Christopher Dupont

Abstract

Engineering microbial cells for the commercial production of biomolecules and biochemicals requires understanding how cells respond to dynamically changing substrate (feast–famine) conditions in industrial-scale bioreactors. Scale-down methods that oscillate substrate are commonly applied to predict the industrial-scale behavior of microbes. We followed a compartment modeling approach to design a scale-down method based on the simulation of an industrial-scale bioreactor. This study uses high cell–density scale-down experiments to investigate *Escherichia coli* knockout strains of five major glucose-sensitive transcription factors (Cra, Crp, FliA, PrpR, and RpoS) to study their regulatory role during glucose oscillations. RNA-sequencing analysis revealed that the glucose oscillations caused the down-regulation of several stress-related functions in *E. coli*. An in-depth analysis of strain physiology and transcriptome revealed a distinct phenotype of the strains tested under glucose oscillations. Specifically, the knockout strains of Cra, Crp, and RpoS resulted in a more sensitive transcriptional response than the control strain, while the knockouts of FliA and PrpR responded less severely. These findings imply that the regulation orchestrated by Cra, Crp, and RpoS may be essential for robust *E. coli* production strains. In contrast, the regulation by FliA and PrpR may be undesirable for temporal oscillations in glucose availability.

Keywords: *Escherichia coli*, industrial-scale, transcriptome, high cell–density, iModulons

---

Significance Statement

This study focused on answering the question of how different strains of *Escherichia coli*, a common microbial host for commercial production of biomolecules and biochemicals, respond to glucose gradients in industrial-scale bioreactors. We apply a scale-down method with oscillating glucose conditions and RNA-sequencing analysis, thus integrating the disciplines of bioprocess development and systems biology. Our study reveals a surprising cellular response to industrial-scale conditions, namely the transcriptional down-regulation of stress-related functions. Additionally, our results signify the importance of using high-throughput scale-down systems for the development of high cell–density fermentation processes. We also provide considerations for genetic engineering efforts to design robust *E. coli* production strains.

Introduction

The scale-up of fermentation processes from lab scale to industrial scale presents a major challenge of bioprocess development due to mixing gradients in industrial-scale bioreactors such as glucose, oxygen, and pH gradients. Microbial cells that travel in these bioreactors experience frequent changes in their extracellular environment, which may result in lower biomass formation, higher by-product formation, and lower productivity, ultimately changing the economic viability of the fermentation (1–4). During bioprocess development in well-mixed lab-scale bioreactors, microorganisms experience optimal, homogeneous conditions, resulting in optimal process performance that is hard to replicate at

an industrial scale. To better understand the behavior of the microorganisms under industrial fermentation conditions and to select the optimal production strains under these conditions, scale-down simulators are employed. Scale-down simulators aim to mimic the relevant industrial-scale phenomena (5–8). Common scale-down simulators rely on either the spatial or temporal separation of two or more different metabolic regimes (e.g. glucose limitation and glucose starvation, or oxygen limitation and oxygen excess). The spatial separation of metabolic regime is often achieved by interconnecting two or more reactors with pumps, such as the stirred tank reactor–plug flow reactor (STR–PFR) or the STR–STR system. Alternatively, scale-down simulators

can oscillate feeding and/or aeration to mimic changing metabolic regimes over time (6). Different scale-down simulators have been shown to result in different outcomes, highlighting that the choice of an appropriate scale-down simulator is essential to ensure that results of scale-down experiments can be transferred to industrial scale (9). Computer models describing the interactions between fluid dynamics and microorganisms in industrial-scale bioreactors have been employed to inform the design of realistic scale-down simulators (10–12).

Recently, RNA-sequencing (RNA-seq) has emerged as an efficient method to study the transcriptional state of microbial cell cultures. An investigation of microbial gene regulation in response to relevant bioprocess scenarios (e.g. nutrient limitations, anaerobiosis, and industrial-scale mixing gradients) can help understand microbial cultures and guide the improvement in bioprocess design (13–15). Typically, gene expression data are analyzed by differentially expressed genes (DEGs), but DEG analysis often results in large numbers of DEGs, thereby raising complexity of deducing gene regulation mechanisms. To gain a broader understanding of the transcriptional regulatory network (TRN), DEG analysis can be mapped against regulons, manually annotated sets of genes that are regulated by a specific regulator (16, 17). In contrast to the bottom-up approach of regulons, independent component analysis (ICA) was recently applied to reconstruct the TRN of *Escherichia coli* with a top-down approach from a large, high-quality RNA-seq dataset, resulting in biologically meaningful groups of independently modulated genes, so-called iModulons (18). For new gene expression data, iModulon activity levels can be inferred, enabling a flexible way of comparing and analyzing gene expression data across different conditions (19, 20).

Highly engineered production strains often have distinct phenotypes from wild-type strains. In this study, we explored the interaction between genetic background and industrial-scale conditions. We perturbed the TRN of *E. coli* by deleting the genes of five glucose-sensitive regulators (Cra, Crp, FliA, PrpR, and RpoS). Subsequently, we characterized the knockout strains in scale-down experiments to study *E. coli*'s response to glucose oscillations under the absence of these regulators, aiming to contribute to the understanding of the TRN specifically under industrial-scale fermentation conditions.

Results

Genotype-dependent physiological response of *E. coli* to repeated glucose oscillations

To mimic substrate gradients typically found in an industrial-scale aerobic fed-batch process, we simulated the formation of glucose gradients in a 90-m^3 STR with four Rushton turbines using a compartment model. Based on the compartment model simulation results, we designed an intermittent feeding regime (IFR) scheme, which imposed repeated glucose starvation on *E. coli* (Fig. 1A). The IFR scale-down method was implemented in the Ambr 250 high-throughput bioreactor system, which allowed us to characterize multiple strains under IFR scale-down and non-IFR control conditions simultaneously. The design of the IFR cycles aimed to closely mimic the relative fraction of the two metabolic regimes "limitation" and "starvation" predicted by the compartment model. The final IFR design imposed glucose starvation on *E. coli* repeatedly every 150 s, for 90 s at each repetition (Fig. 1B). The timescale of the oscillations in the IFR design was similar to the ones typically expected in industrial-scale bioreactors, in which cells experience metabolic regime changes at

the timescale of tens of seconds (21). Repeated glucose starvation in scale-down experiments resulted in lower biomass formation and higher CO_2 formation compared with control experiments over time (Fig. 1C). Oscillations of the dissolved oxygen (DO) during the feeding phase in scale-down experiments were due to the oscillating addition of glucose.

The different TF knockout strains had varying effects on the maximum growth rate μ_{max} and biomass yield Y_{SX} of *E. coli* in batch cultures (Fig. 2A). Both the *E. coli* WT strain and the $\Delta prpR$ strain exhibited a μ_{max} of 0.37 h^{-1}. The $\Delta fliA$ and the $\Delta rpoS$ strain showed a minor effect on μ_{max} with values of 0.33 h^{-1}, while the Δcra and the Δcrp strain showed a severe decline of μ_{max} with values of 0.23 h^{-1} and 0.2 h^{-1}, respectively. The WT strain showed a biomass yield Y_{SX} of 0.66 mol$_C$/mol$_C$, meaning that two-thirds of the carbon supplied as glucose was converted to biomass in batch cultures. Compared with the WT strain, the $\Delta prpR$ and the $\Delta rpoS$ strain showed similar average Y_{SX} values of 0.62 mol$_C$/mol$_C$ and 0.64 mol$_C$/mol$_C$, respectively. The $\Delta fliA$ and Δcra strains showed a slightly reduced biomass yield with Y_{SX} values of 0.59 mol$_C$/mol$_C$ and 0.55 mol$_C$/mol$_C$, respectively. The Δcrp strain grew with markedly higher $Y_{SX} = 0.78$ mol$_C$/mol$_C$ in batch cultures, compared with the WT strain.

The difference in the formation of the major carbon products biomass and carbon dioxide (CO_2) between scale-down and control experiments was assessed by comparing the carbon yields on glucose (Fig. 2B, C). The yield of biomass on glucose Y_{SX} and the yield of CO_2 on glucose Y_{SC} over the entire fermentation were 0.58 and 0.47, respectively, in scale-down cultures of the WT strain. Compared with $Y_{SX} = 0.62$ and $Y_{SC} = 0.42$ in control cultures of the WT strain, Y_{SX} was significantly lower and Y_{SC} was significantly higher in scale-down cultures. The biomass yield Y_{SX} was significantly lower in scale-down cultures compared with control cultures for the TF knockout strains $\Delta prpR$ and $\Delta rpoS$ (Fig. 2B). The comparison of Y_{SC} between scale-down and control showed that for all strains except the Δcra and $\Delta fliA$ strain, Y_{SC} was significantly higher in scale-down cultures (Fig. 2C). The two-factor ANOVA tests showed that both design factors (cultivation condition and genotype), as well as the design factor interaction, had a significant impact on Y_{SX} and Y_{SC}. Most importantly, this proved that the physiological response to repeated glucose starvation was genotype dependent.

Transcriptional response of *E. coli* to repeated substrate availabilities

The transcriptional response of the different *E. coli* strains to scale-down was initially assessed by DEGs between scale-down and control cultures based on RNA-seq samples taken at the end of each fermentation. An analysis of DEGs with volcano plots (see Fig. S10) and a statistical enrichment of clusters of orthologous groups (COGs) (see Table S2) were performed. At the end of the scale-down fermentations compared with the control fermentations of the *E. coli* WT strain, 94 genes were down-regulated and 81 genes were up-regulated (Fig. 3A). Particularly, the knockout strains Δcra (311 up-regulated, 151 down-regulated), Δcrp (177 up-regulated, 147 down-regulated), and $\Delta rpoS$ (52 up-regulated, 154 down-regulated) showed a more sensitive response to scale-down, with a higher number of up- and/or down-regulated DEGs than the WT strain. The $\Delta fliA$ (43 up-regulated, 65 down-regulated) and $\Delta prpR$ (62 up-regulated, 60 down-regulated) showed a less sensitive response to scale-down, with fewer up and down-regulated DEGs than the WT strains. Among the DEGs of all tested *E. coli* strains, we found a surprisingly large
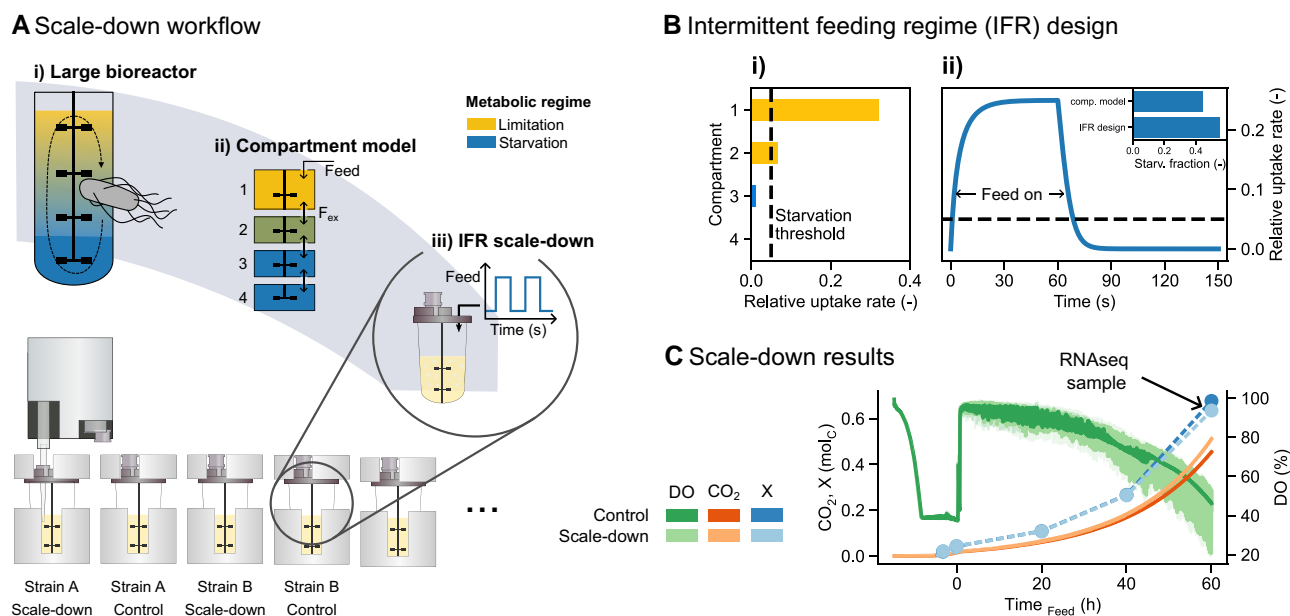
Fig. 1. A high-throughput scale-down approach. A) A schematic workflow to characterize the response of multiple strains to industrial-scale carbon oscillations based on the compartment model approach. Scale-down experiments were implemented in the Sartorius Ambr 250 high-throughput system. A 90-m³ stirred tank reactor with four Rushton turbines (i) was modeled with four compartments (ii) to derive the IFR design implemented in the Sartorius Ambr 250 HTP system (iii). B) The metabolic regime classification was based on the relative substrate uptake rate q_S/q_{Smax} (limitation: $q_S/q_{Smax} \geq 0.05$, starvation: $q_S/q_{Smax} < 0.05$) (i). A feed pulse was designed to match the relative time spent in starvation (starv. fraction) between the compartment model solution and the IFR scale-down (ii). C) In fed-batch experiments of an *E. coli* wild-type strain, the IFR scale-down resulted in lower biomass, higher CO_2, and higher O_2 consumption. The black arrow indicates the timepoint at which samples for RNA-seq were taken. Complete time profiles from fed-batch experiments available in Supplementary Information (Figs. S3–S5 and S7–S8).

number of unique genes that were differentially expressed in one strain, but none of the others (highlighted DEGs in Fig. 3A). In particular, the Δ*cra* and Δ*rpoS* strains showed a large amount of unique up- and down-regulated genes. Overall, the DEGs of all tested strains consisted of a considerable share of unique DEGs (up-regulated DEGs: 14% in WT, 41% in Δ*cra*, 58% in Δ*crp*, 12% in Δ*fliA*, 31% in Δ*prpR*, and 35% in Δ*rpoS*; down-regulated DEGs: 5% in WT, 42% in Δ*cra*, 16% in Δ*crp*, 18% in Δ*fliA*, 12% in Δ*prpR*, and 40% in Δ*rpoS*).

In the *E. coli* WT strain, the transcription factors of interest were all statistically enriched among the DEGs between control and scale-down cultures, highlighting that these transcription factors indeed play a role in the regulatory response to industrial-scale fermentation conditions (Fig. 3B). Genes controlled by Cra and PrpR were statistically enriched among the up-regulated DEGs in the parent strain, while genes controlled by Crp, RpoS, and FliA were significantly enriched among the down-regulated genes. The response to repeated scale-down with respect to the transcription factors of interest was changed in the *E. coli* knockout strains. Compared with the parent *E. coli* strain, the Δ*cra* strain did not show statistically enriched DEGs controlled by CRP and PrpR, in the Δ*crp* strain, enrichment of genes controlled by Cra, FliA, and PrpR was lost, in the Δ*fliA* strain, FliA enrichment was lost, and the CRP enrichment was found in the up-regulated DEGs (opposite to the parent strain). The Δ*prpR* strain did not show enrichment of genes controlled by PrpR and σ^F, and in the Δ*rpoS* strain, the enrichment of genes controlled by RpoS was reversed compared with the parent strain and was now found among the up-regulated DEGs. Taken together, the gene expression analysis indicated that the transcriptional regulation in response to oscillating glucose availabilities was highly genotype dependent.

iModulons analysis reveals regulatory biomarkers of *E. coli* under industrial-scale glucose oscillations

In addition to the typical approach of analyzing DEGs, we analyzed the transcriptional data from our experiments using iModulons, which are statistically independent components comprised of co-modulated genes in *E. coli*. In contrast to manually annotated regulons, iModulons are computed using ICA on gene expression data from a sufficiently large dataset containing samples taken under a variety of conditions. Many of these components have been tied to known regulons identified through experimental binding sites (18, 19). We inferred iModulon activities for our samples from the public database PRECISE-1K, which contains more than 1,000 *E. coli* samples. The calculated iModulon activities enabled us to quantitatively compare gene expression across several conditions at once and contextualize them with other samples from PRECISE-1K. The biological functions associated with the iModulons facilitated explaining the state of the TRN under glucose oscillation conditions.

The RpoS iModulon was the independent component with the largest share of explained variance (>11%) within our dataset (Fig. 4A). Other iModulons in the system category of stress responses (shown in orange) that showed high explained variance were the iModulons GadXW, Capsule, Curli-1 and 2, and FlhDC-2. High values of the explained variance in the iModulons Crp-1, and 2, and crp KO-1 that are in the system category of metabolism (shown in blue) can be attributed to samples from cultures of the Δ*crp* strain in our data. To elucidate which elements of the TRN had responded to glucose oscillations, we performed differential iModulon activity (DiMA) analysis. iModulons highlighted in Fig. 4B–G were differentially activated between scale-down and control cultures of the tested *E. coli* strains. The total
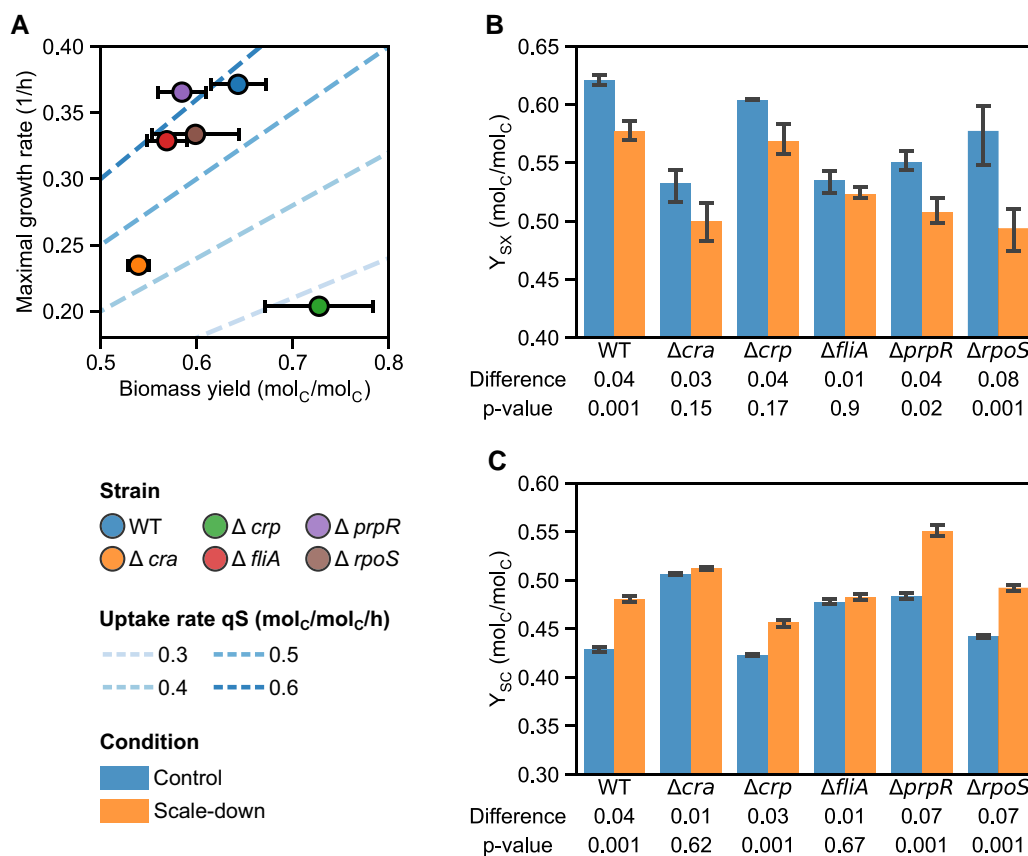
Fig. 2. Condition-dependent growth physiology of the tested *E. coli* strains. A) During the initial batch phase, the transcription factor knockouts impacted the maximal growth rate $\mu_{\max}$ and the biomass yield Y_{SX}. The dashed contour lines indicating constant values of the biomass-specific glucose uptake rates q_S computed by the formula $q_S = \mu/Y_{SX}$. Slopes of the contour lines are equal to q_S. Comparison of the specific acetate formation rate q_A available in Supplementary Information (Fig. S6). B) During the feeding phase, the biomass yield on consumed glucose Y_{SX} was generally lower in scale-down cultures compared with control cultures. C) During the feeding phase, the CO_2 yield on consumed glucose Y_{SC} was generally higher in scale-down cultures. Yields were calculated based on the carbon molar amounts of net formed products and net consumed substrate between the start and the end of the feeding phase, excluding the initial batch phase. To calculate the carbon moles of biomass, the molecular weight 24.6 g/mol$_C$ based on the molecular formula of biomass $CH_{1.8}O_{0.5}N_{0.2}$ was used (22). Complete time profiles of net formed biomass and CO_2 and net consumed glucose are provided in Supplementary Information (Figs. S3, S4 andS7). P-values of the (absolute) difference between scale-down and control cultures were calculated by two-factor ANOVA tests.

number of DiMAs was comparable to the total number of DEGs (Fig. 3A). For example, the Δ*cra* strain, which showed the most DEGs, also showed the most DiMAs (Fig. 4C), and the Δ*fliA* strain showed the least amount of both DEGs (Fig. 3A) and DiMAs (Fig. 4E). Across all DiMAs, the highest absolute differential activities were found in the Capsule iModulon (functional category: extracellular structures), which was differentially activated in the Δ*cra*, Δ*crp*, and Δ*rpoS* strain (Fig. 4C, D, G). Other iModulons with high absolute DiMAs were EvgA, and GadXW (functional category: envelope stress), FlhDC-2 (functional category: extracellular structures), RpoS (functional category: global stress), Putrescine (functional category: nitrogen metabolism), and Fur-2 (functional category: metal homeostasis) (Fig. 4H).

The activities of the RpoS iModulon, which captures the general stress response in *E. coli*, were elevated in all strains, except the Δ*rpoS* strain (Fig. 5B). *E. coli* activates the general stress response when transitioning into stationary phase or growing under nutrient limitation (23). In fact, PRECISE-1K samples taken from chemostat or fed-batch cultures show higher RpoS activities compared with samples from batch cultures (Fig. S11). The scale-down cultures of the Δ*cra* and the Δ*crp* strain showed a significantly reduced RpoS activity compared with their control cultures, which indicates a lowered general stress response in scale-down cultures of these strains. The stringent response, mediated by the

alarmone (p)ppGpp, is closely related to the RpoS-dependent general stress response in *E. coli* (24). When *E. coli* becomes deficient in amino acids, the blocking of ribosomes by uncharged tRNA leads to (p)ppGpp synthesis (25, 26). Therefore, the stringent response in *E. coli* is initiated by a broad range of nutrient limitations and primarily by amino acid starvation (27). *E. coli* is known to initiate the stringent response during carbon-limited fed-batch (23, 28), which was suggested to be due to low amino acid pools indirectly caused by a low availability of precursor molecules (24). The fed-batch samples of recent high cell–density studies (project names in PRECISE-1K "DDB2" and "DDB3") show significantly lower ppGpp iModulon activities than samples from those studies taken during the batch phase (Fig. S12); hence, activities of the ppGpp iModulon decrease when the stringent response is onset. The low ppGpp iModulon activities measured in our study (Fig. 5A) confirm that the stringent response was likely initiated in the control fed-batch cultures, which can be explained by the relatively low growth rate of $\mu = 0.05 \text{ h}^{-1}$ during all fed-batch cultures in this study. Therefore, we observed no further increase in the stringent response in scale-down cultures, since the stringent response was already initiated under the control condition.

The alarmone cyclic AMP (cAMP) is formed in *E. coli* under conditions of low glucose availability (e.g. during fed-batch) and binds to the regulator protein Crp. The iModulon Crp-2 consists of genes
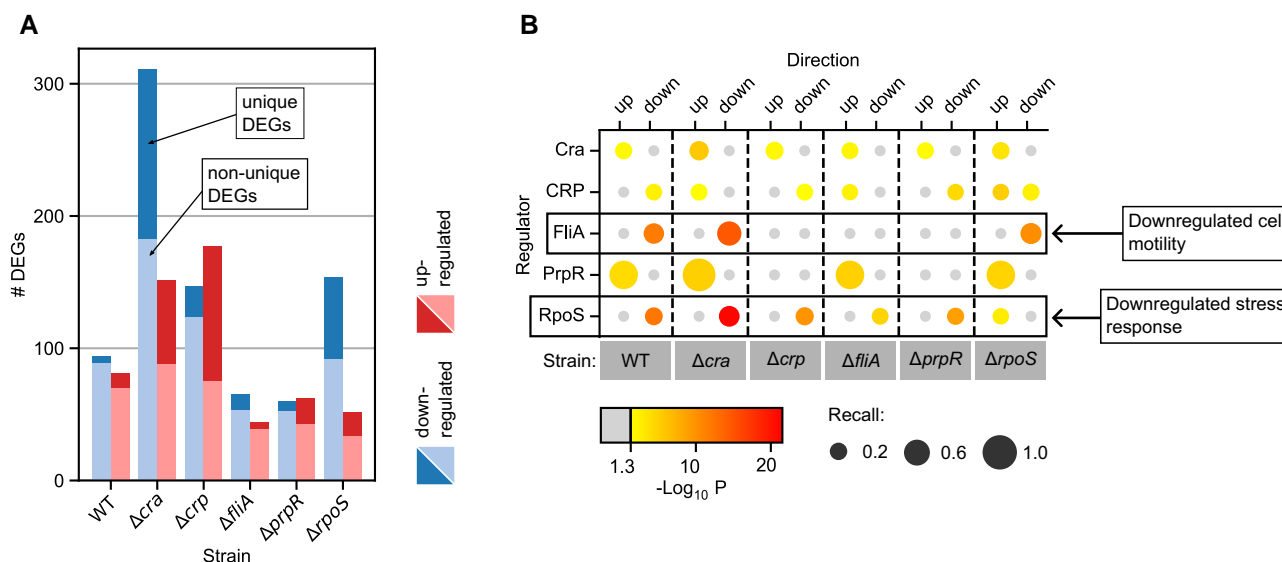
Fig. 3. An overview of DEG analysis in scale-down conditions with oscillating glucose. For the DEGs, a threshold of log2 fold change ±0.58 (corresponding to 1.5, meaning a 50% decrease/increase) and adjusted *P*-value <0.05 were applied. A) The number of DEGs between scale-down and control cultures of all tested strains. The highlighted portions of the bars (darker color) indicate genes that were only found among the up- or down-regulated DEGs of this strain and none of the other strains. B) Statistical regulon enrichment of the knocked-out regulators among the scale-down DEGs based on RegulonDB (threshold *P* < 0.05). The color scale indicates the significance of the statistical enrichment (negative log10 *P*-value shown; low number = less significant, high number = more significant). Regulators without significant enrichment are shown in gray. The size of the data points indicates the regulon recall. Recall = #DEGs in Regulon/# total genes in regulon.

regulated by Crp-cAMP, for example, genes related to the transport and catabolism of alternative carbon sources. The Crp-2 iModulon activities were consistently high in all samples, except the Δ*crp* strain, confirming that the cAMP-dependent response was initiated (Fig. 5C). As shown previously, the iModulons RpoS and Crp-2 are not only biomarkers of *E. coli*'s growth phenotype but also clearly indicate the knockouts of their respective transcription factor. The same is true for the iModulon Cra, which showed a significantly increased activity in cultures of the Δ*cra* strain (Fig. S13), due to the absence of Cra-dependent repression of positively weighted genes and absent activation of negatively weighted genes in the Cra iModulon.

The Propionate iModulon consists of a single operon (*prp* genes of the methyl citrate cycle), which is activated by PrpR. The Propionate iModulon activity was significantly reduced in the Δ*prpR* strain, due to the absence of PrpR-dependent transcriptional activation. Additionally, the Propionate iModulon was also down-regulated in the Δ*crp* and the Δ*rpoS* strain (Fig. 5D). Crp directly activates the *prpRp* promoter (EcoCyc.org), which explains the inactivation of the Propionate iModulon in the Δ*crp* strain. A down-regulation of the methyl citrate cycle was also previously reported in *E. coli* strains lacking RpoS; however, the underlying mechanisms remain unclear (29). Although the expression of the regulator gene *fliA* was absent in the Δ*fliA* strain (Fig. S14), the activities of the FliA iModulon (Fig. 5F) did not clearly indicate a *fliA*-knockout phenotype, especially when compared with the other strains studied. This observation implies that the FliA iModulon captures a more complex regulatory mechanism, and while many of its genes are regulated by FliA, their transcription is likely not solely reliant on FliA.

Reduced cell motility expression and down-regulated stress-related functions under glucose oscillations

The iModulons FlhDC-1 and FlhDC-2 capture the expression of the flagellar system in *E. coli*. The transcription factors FliA and FlhDC

activate most genes in these two iModulons (Fig. 5E). Crp exhibits an indirect control over FlhDC-1 and 2 by activating the expression of the regulator genes *flhC* and *flhD*. Consistently, the FlhDC-2 iModulon activity was the lowest in the Δ*crp* strain. The activities of FlhDC-1 and FlhDC-2 were reduced in the Δ*fliA* strain and surprisingly in the Δ*prpR* strain as well. No direct connection between the regulator PrpR and the down-regulation of flagellar gene expression is known. While the flagellar gene expression was already low in the Δ*fliA* and the Δ*prpR* strain, the iModulon activities of FlhDC-2 further reduced in response to scale-down. The down-regulation of cell motility in response to scale-down was most prominent in the Δ*cra* and the Δ*rpoS* strain (both of which had the highest iModulon activities in control cultures) as well as in the WT strain.

Several iModulons in PRECISE-1K capture responses to different stresses in *E. coli*. During scale-down experiments with glucose oscillations, DO control was switched off and the reactor stirring speed and aeration rate were set to constant values of 4,000 rpm and 0.25 Lmin^{-1}, respectively (see Materials and methods section). Under these conditions of oscillating glucose feeding fed-batch phase, the iModulon activity of the regulators ArcAB and Fnr was found to be not differentially activated between the scale-down and control cultures of all strains tested from the DiMA analysis (Fig. 4B–G) and differential gene expression (DGE) analysis (Fig. S10), since the DO values (Fig. S8) did not decrease below 20% and reach microaerobic conditions. The iModulons Fur-1 and Fur-2 primarily describe iron homeostasis and capture different parts of the Fur regulon (Fig. 5G, Venn diagram). As a result of redox/oxidative stress, reactive oxygen species (ROS) damage iron-containing enzymes (30–32). Therefore, the Fur regulon can also be seen as a biomarker of redox/oxidative stress (20). Fur represses genes related to iron uptake when binding to intracellular Fe^{2+}. When *fur* is knocked out in *E. coli*, the activities of both Fur iModulons show the highest values observed across PRECISE-1K, due to the absence of Fur-dependent repression, while growth in iron-rich media such as LB generally results in very low Fur-1/2
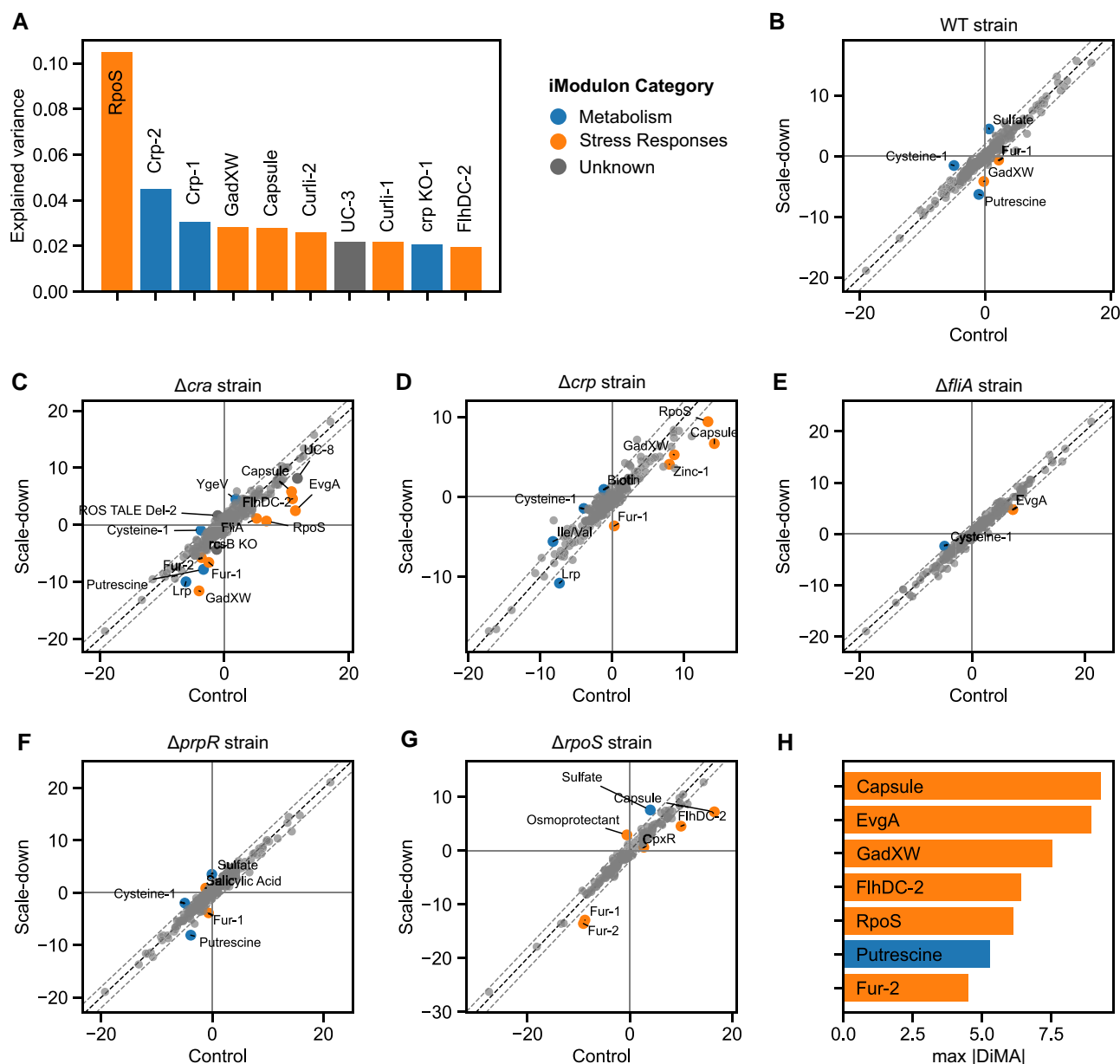
Fig. 4. An analysis of independent component (iModulon) activities inferred from the *E. coli* iModulon database PRECISE-1K. A) iModulons with the highest explained variance within the dataset of this study. System category of the iModulons indicated by the color of the bar. B–G) DiMA plots between scale-down and control cultures of the WT strain and the five TF knockout strains. Highlighted iModulons are considered differentially activated. For DiMAs, a threshold of ±2 and a FDR of <0.1 were applied. H) iModulons with the overall highest absolute DiMA across all DiMA plots.

iModulon activities (annotations in Fig. 5G). Fur-1 and Fur-2 are also indirectly linked to redox stress in *E. coli* (20, 33). For example, samples in PRECISE-1K of an *E. coli* wild-type strain grown in batch cultures where 250 μM of the ROS-generating agent Paraquat was added showed an increase in the Fur-1 and Fur-2 iModulons (annotation in Fig. 5G). ROS can cause Fenton chemistry (oxidation of Fe^{2+} to Fe^{3+}), which can cause a lower repression by Fur since less Fe^{2+} is bound to Fur (34, 35). Both Fur-1 and Fur-2 showed a reduced activity in response to scale-down (Fig. 5G), indicating lower redox stress compared with control cultures. The Δ*cra* and the Δ*rpoS* strain displayed the most sensitive response to scale-down compared with their control cultures, while the iModulon activities of Fur-1 and Fur-2 did not change in the Δ*fliA* strain, suggesting that the redox state of *E. coli* was not perturbed in this strain. The Cysteine-1 iModulon consistently increased in

samples of scale-down cultures compared with control cultures (Fig. 5H). An increase in the Cysteine-1 iModulon has been linked to lower redox stress in *E. coli* (20).

The iModulons GadXW (related to glutamate-dependent acid resistance and envelope stress) and *rcsB* KO (formerly called GadEXW in PRECISE 2.0 are related to envelope stress) show a strong correlation across the samples of PRECISE-1K, as well as in samples from our study (Fig. 5I). PRECISE-1K samples of *E. coli* knockouts of the related regulator genes (*gadX*, *gadW*, the master regulator *gadE*, and rcsB) are annotated in Fig. 5I. Both iModulons activities reduced in response to scale-down, with the Δ*cra* strain showing the most sensitive down-regulation, indicating a lowering of acid and envelope stress. Notably, the Δ*fliA*, Δ*prpR*, and Δ*rpoS* strains showed low iModulon activities in both GadXW and *rcsB* KO, indicating a lower baseline stress response, while
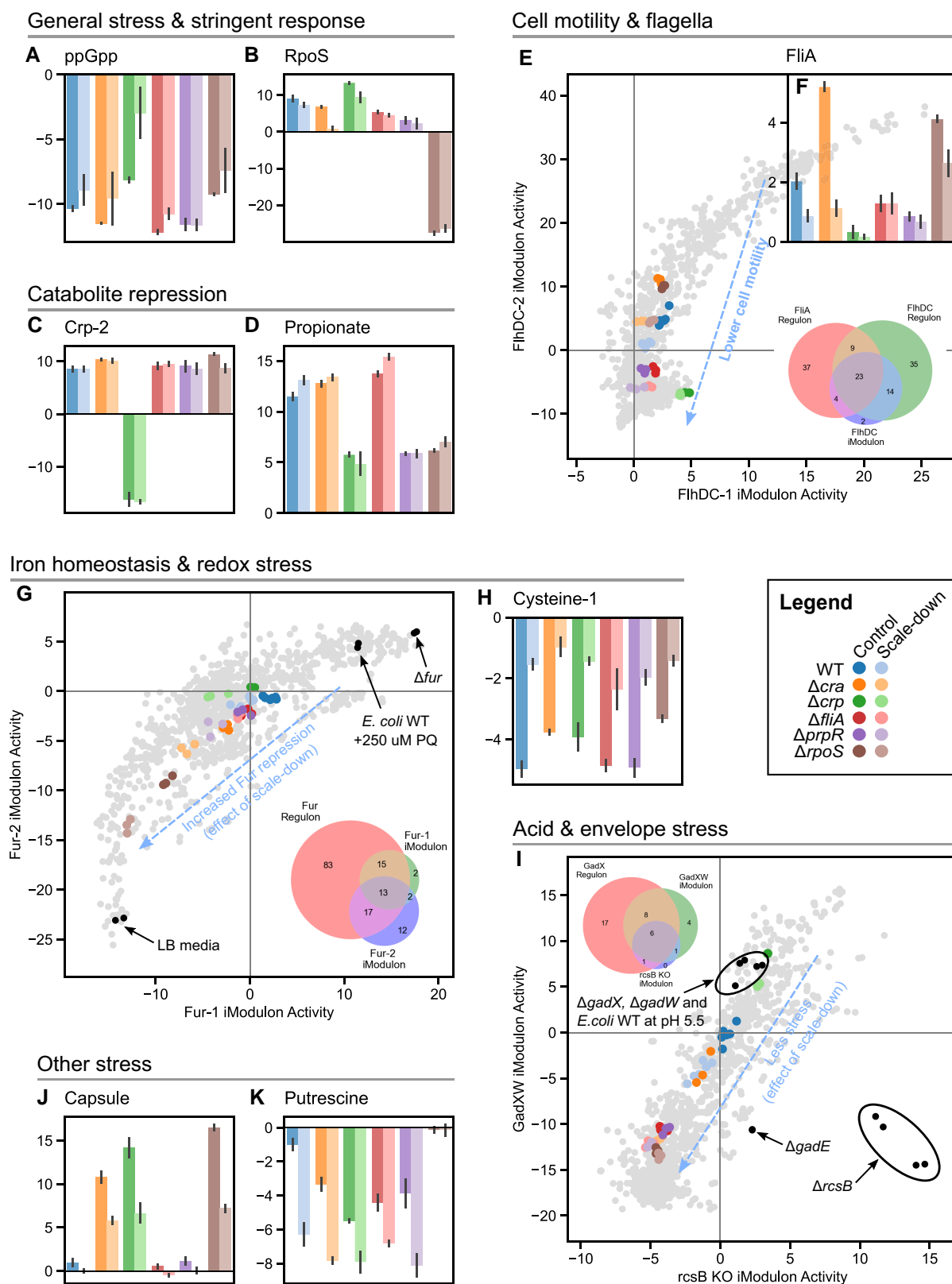
Fig. 5. Activities and relationships between selected iModulons grouped by their relevant functions. The bar plots (A–D; F; H; J–K) showing iModulon activities of all strains under scale-down and control conditions. Phase portraits comparing the activities of iModulon pairs FlhDC-1 and FlhDC-2 (E), Fur-1 and Fur-2 (G), and GadXW and rcsB KO (I), where the gray data points indicate the iModulon activities of all samples in PRECISE-1K.

the stress responses were activated in the Δ*crp* strain. The Capsule iModulon captures colanic acid capsule biosynthesis in *E. coli*. Colanic acid, an exopolysaccharide secreted by *E. coli*,

encapsulates the organism, providing protection and promoting biofilm formation when exposed to stressful conditions (36–38). In our study, we found that the Capsule iModulon was activated

in the knockout strains of *cra*, *crp*, and *rpoS* (Fig. 5J). However, under scale-down conditions, the Capsule activity was significantly reduced in these strains, indicating that under scale-down conditions, the stress response captured by the Capsule iModulons was reduced. The Putrescine iModulon contains the genes involved in putrescine transport and catabolism. Putrescine catabolism has been linked to *E. coli*'s response to several stresses (39). The activity of the Putrescine iModulon reduced in response to scale-down, indicating a lower stress response in all strains, except Δ*rpoS*, where the Putrescine iModulon activity was at a constantly higher level (Fig. 5K).

Discussion

This study presents *E. coli*'s response to industrially relevant glucose oscillations. The responses were illustrated by knocking out glucose-sensitive transcriptional regulators and growing the *E. coli* strains in two different conditions, i.e. with continuous glucose feed (control condition) and with intermittent glucose feed representing temporal industrial-scale substrate gradients (scale-down condition). The scale-down and control cultures were compared with each other and showed that the growth physiology was impacted not only by the cultivation conditions but also by the strain genotype. By applying iModulon analysis, we identified that *E. coli* responds to repeated substrate oscillations by down-regulating stress-related and cell motility functions. The selection of relevant gene knockout targets was inspired by the work of Löffler et al. (13), who found that genes controlled by Cra, Crp, FliA, PrpR, and RpoS had been differentially expressed in response to prolonged periods of repeated glucose starvation in a STR–PFR scale-down setup.

Of the above-mentioned regulator genes, the gene *cra*, transcribing the "catabolite repressor activator" Cra, and the gene *crp*, transcribing the cAMP receptor protein Crp, were selected as suitable knockout targets to study under glucose oscillations, as they are key regulators of central carbon metabolism responding to changing carbon availability (24). Cra activates genes involved in gluconeogenesis, the TCA cycle, and the glyoxylate shunt and deactivates genes related to the Entner–Doudoroff pathway, and glycolysis (40, 41). The regulation mediated by Cra is counteracted by fructose-1,6-bisphosphate, so that Cra-dependent gene regulation predominantly occurs when carbon availability is low (42). *E. coli* mutant strains lacking *cra* are unable to grow on gluconeogenic substrates such as acetate, pyruvate, and lactate (41, 42). Crp is activated when bound to the alarmone cAMP, which is synthesized by the adenylate cyclase Cya in response to limited glucose availability (24). The cAMP–Crp complex mediates the catabolite repression in *E. coli*. Genes responsible for the uptake of alternative carbon sources and the expression of high-affinity uptake systems are activated by cAMP–Crp (29). Therefore, *E. coli* mutants that lacked *crp* were unable to utilize alternative carbon source and exhibited a reduced glucose affinity in glucose-limited chemostat cultures (29). Additionally, cAMP–Crp positively regulates genes of the TCA cycle genes and negatively regulates genes of the glyoxylate shunt (24, 43).

Furthermore, the genes *fliA* and *rpoS*, transcribing the alternative sigma factors FliA (σ^F) and RpoS (σ^S), respectively, were identified as knockout targets for this study. Both sigma factors were shown to control genes that were differentially expressed in response to repeated glucose starvation (13). FliA is required for the expression of genes involved in motility and flagellar synthesis, as well as biofilm formation (44). Among genes that were differentially expressed in response to repeated glucose starvation,

fliA, and other genes controlled by FliA, were identified as some of the most energy-demanding genes for transcription and translation in *E. coli* (13). RpoS regulates the general stress response in *E. coli* which can be triggered by nutrient limitation, when *E. coli* enters the stationary phase, and by a wide array of stresses (23). Löffler et al. (13) reported that in response to repeated glucose starvation, the general stress response was up-regulated in *E. coli*; however, earlier reports implied a down-regulation of RpoS-controlled gene expression under industrial cultivation conditions (45, 46), which led us to investigate how a Δ*rpoS* mutant strain would respond to repeated glucose starvation in our scale-down experiments.

Lastly, we selected the regulator PrpR as knockout target, which together with the cAMP–Crp complex acts as activator of the *prp* operon (EcoCyc.org). The genes *prpBCDE* in *E. coli* express the methyl citrate cycle, which is required for propionate catabolism (47), and showed a strong upregulation in response to repeated glucose oscillations in the work of Löffler et al (13). We therefore investigated how a Δ*prpR* mutant strain of *E. coli* lacking the methyl citrate cycle would respond to repeated glucose starvation.

The Δ*cra* and Δ*crp* transcriptional factor knockout strains under the conditions tested showed a significant impact on the growth physiology during the batch phase of cultivation, observed from their biomass-specific glucose consumption rates which decreased by about 25 and 50%, respectively, in comparison with the parent *E. coli* strain. In the case of the Δ*crp* strain, a trade-off between growth rate and biomass yield was observed, which is a common phenomenon in the physiology of microbial growth (48). While growing at a lower growth rate, the Δ*crp* strain exhibited a lower specific acetate formation rate, resulting in a low amount of acetic acid formation relative to formed biomass (Fig. S6). A reduced growth rate of *crp* mutant *E. coli* strains was also previously observed (49). However, the same trade-off was not observed in the Δ*cra* strain, which also grew at a lower growth rate in the batch phase but showed a higher specific acetate formation rate resulting in a higher amount of acetic acid relative to formed biomass (Fig. S6). In *E. coli*, formation of acetic acid via Pta-Ack and consumption via Acs occur simultaneously (50). Down-regulation of the *acs* gene has previously been linked to low expression of Cra; hence, the net formation of acetic acid may have been higher during the batch phase in the Δ*cra* strain, due to a reduced Acs-dependent consumption of acetic acid (50). Formation of overflow byproducts often correlates with fast growth; however, the maximal growth rate of the Δ*cra* strain cultures could have been inhibited by high organic acid concentrations (48, 51). In fact, acetate formation in *E. coli* K-12 strains lacking Cra was previously reported to inhibit growth (52).

In scale-down cultures, we found that the growth phenotypes of the tested *E. coli* strain trended toward lower biomass (significant Y_{SX} differences observed in the WT, Δ*prpR*, and Δ*rpoS* strain) and higher CO_2 formation (significant Y_{SC} differences observed in the WT, Δ*crp*, Δ*prpR*, and Δ*rpoS* strain) in comparison with the control condition. Löffler et al. (13) estimated that frequent on-and-off switching of transcription and translation could cause up to 40–50% higher energy demand in *E. coli* under glucose oscillations. A higher energy demand would require *E. coli* to use more carbon for the generation of energy and less carbon for growth and therefore an increased maintenance requirement, which was confirmed in STR–PFR scale-down experiments (53). Lower biomass concentrations were also reported when *E. coli* was exposed to glucose oscillations (45). Interestingly, the growth phenotype of the Δ*fliA* strain showed the least impact of scale-down conditions. Cell motility is an expensive function in *E. coli*.

Löffler et al. (13) suggested a list of 20 highly energy-demanding genes as knockout targets, out of which 5, including *fliA* itself, are directly controlled by FliA, to reduce the additional energy cost caused by the undesired expression of these genes under glucose oscillations. Therefore, the knockout of *fliA* may have contributed to the more stable *E. coli* phenotype in our experiments. However, in the parent *E. coli* strain, we observed that the genes controlled by FliA were significantly enriched among the down-regulated genes; because, unlike the large-scale industrial fermentation, the scale-down experiments performed in this study capture only the temporal gradient of nutrient availability and not the spatial gradient, where there will be a high necessity for motility regulation using FliA in the case of starved condition. The largest decline in biomass formation was observed in scale-down cultures of the Δ*rpoS* strain. Keeping the trade-off between RpoS and FliA in mind, the expression of energy-expensive genes indirectly repressed by RpoS and directly activated by FliA may have caused a higher added maintenance demand of the Δ*rpoS* strain in scale-down cultures (54). In fact, as the analysis of DEGs (Fig. S9) showed, genes controlled by FliA were significantly enriched among the up-regulated genes in the Δ*rpoS* strain.

Compared with the parent strain, we found more DEGs between scale-down and control cultures of the Δ*cra*, Δ*crp*, and Δ*rpoS* strains. The lack of these regulator genes seemed to result in a more sensitive response of *E. coli*'s transcriptional regulation to glucose oscillations, which may be an important consideration for the engineering of *E. coli* production strains. In contrast, the Δ*fliA* strain showed the least amount of DEGs between scale-down and control cultures (Fig. 3A), which was in line with our observations made based on growth physiology (Fig. 2). We also observed a surprisingly large amount of unique DEGs (genes that were differentially expressed in response to scale-down by only one of the tested strains), showing that the transcriptional response was genotype dependent, and scale-down results obtained from experiments with wild-type strains therefore have potentially limited applicability for industrial processes (13, 45, 55, 56).

Despite the large number of unique DEGs, the DGE analysis also showed common patterns. In most tested strains, FliA-regulated genes and RpoS-regulated genes were down-regulated (Fig. 3B). The down-regulation of genes controlled by RpoS was a surprising finding since the RpoS-mediated general stress response is generally associated with lack of nutrients. Furthermore, this observation differs from the previous study, where an increase in the general stress response under scale-down conditions was observed (13). On the other hand, Enfors et al. (45) observed an increase in cell viability in response to scale-down, where glucose oscillations occurred at very low average growth rates and shorter timescales. The DiMA analysis (Fig 4B–H) also showed other stress-related iModulons (e.g. Fur-1/2, GadXW, EvgA, RpoS, FlhDC-2, Capsule) less activated during scale-down cultivations.

The iModulon ppGpp is a biomarker of the alarmone (p)ppGpp (mediating the stringent response), while the iModulon Crp-2 is a biomarker of cAMP (activating Crp under glucose limitation). The activities of both iModulons indicated that the (p)ppGpp-mediated stringent response and cAMP–Crp-dependent gene regulation were likely activated in our control cultures (Fig. 5A, C). In fed-batch cultivations of *E. coli*, both alarmone concentrations increased at the onset of the fed-batch phase (24). Löffler et al. (13) also measured a fast increase in the cellular (p)ppGpp content in *E. coli* after entering the glucose starvation compartment of their scale-down reactor. We suspect that rather than repeated starvation, repeated periods of higher glucose availability were the dominant effect of the IFR scale-down cycles resulting in a temporary

down-regulation of (p)ppGpp and cAMP biosynthesis, which may explain why we observed an overall reduced stress response in scale-down cultures. The RpoS iModulon activities trended lower in response to scale-down and especially the Δ*cra* strain showed a significant down-regulation of the iModulon (Fig. 5B). iModulons related to redox stress (Fur-1/2 and Cysteine-1), acid and envelope stress (GadXW and rcsB KO), and other stresses (Capsule and Putrescine) were in line with the general observation of a lower stress response under scale-down conditions.

The Propionate iModulon showed minor upregulation in response to scale-down, however, not as clear as the statistical enrichment of PrpR-regulated genes among the up-regulated DEGs of the WT, Δ*cra*, Δ*fliA*, and Δ*rpoS* strain (Fig. 3B) suggested. Löffler et al. (13) also observed an upregulation of the propionate catabolism in scale-down conditions (Fig. S17). It remains unclear why *E. coli* up-regulates the methyl citrate cycle. The knockout of *prpR* surprisingly also resulted in lower expression of cell motility genes (FlhDC-2 and FliA iModulons). A direct link between PrpR and the genes related to cell motility is not known from our study. This observation highlights that PrpR and the methyl citrate cycle might play a major role under conditions of glucose limitation and temporal oscillations in glucose availability prevalent in industrial-scale high cell–density fermentations. However, to further understand the mechanism of PrpR regulation, additional research is required with propionate producing recombinant *E. coli* strains. We observed a down-regulation of genes and iModulons related to cell motility. Particularly, the activities of FlhDC-2 (Fig. 5E) and FliA (Fig. 5F) showed that the expression of cell motility genes was activated the most in control cultures of the Δ*cra* and the Δ*rpoS* strain. However, both strains also showed the strongest down-regulation of these iModulons in response to scale-down conditions.

Overall, through systematic transcriptional analysis, we reported that *E. coli* responds to glucose oscillations by exhibiting a "less stressed" transcriptional phenotype by down-regulating several stress-related and cell motility functions under industrial-scale conditions. Furthermore, we found that the response to glucose oscillations was genotype dependent. This calls for high-throughput scale-down methods such as the one presented in this study to be integrated in early bioprocess development to characterize candidate production strains under industrial-scale conditions and integrate their responses in the design of robust cell factories.

In this study, we have focused on analyzing the long-term change of the transcriptome of different strains in response to repeated glucose starvation from an experimental setup where the culture conditions were maintained constant over time, especially with respect to growth rate in an exponential fed-batch cultivation. Based on the research done by Löffler et al., where a new transcriptional steady state was reached after about 24 h in chemostat fermentations, we expect that the expression data reported in this study represents new transcriptional steady state that *E. coli* cells have adopted after long exposure to repeated glucose starvation intervals (13). While this study focused on understanding the long-term TRN response from RNA-seq data, care must be taken explicitly to illustrate post-transcriptional, translational, and metabolic regulation mechanisms happening under one glucose oscillation. Further research in this direction can be aimed by obtaining additional level of omics data (e.g. phosphoproteome, intracellular metabolome, metabolic pathway fluxes or enzyme activities) with dynamic time resolution during the short-term transition from glucose excess to glucose starvation for the WT and KO strains. In recent work, Gecse (57) performed comprehensive proteome analysis with 2′ fucosyllactose-producing *E. coli* strain in glucose oscillation-based scale-down

experiments and observed down-regulation of several stress response associated proteins, which is in line with the observations made in this study with iModulon analysis. On metabolome level, a study with labeled glucose has shed insights into the activation of parallel glycolysis, i.e. the Entner–Doudoroff pathway when *E. coli* was subjected to repeated glucose upshifts (58).

Materials and methods

Bacterial strains

In total, six different *E. coli* strains (Table 1), including five transcription factor knockout strains and one parent strain (control), were tested in IFR scale-down and continuously fed control fed-batch cultures (59). The knockouts were introduced using methods described previously (60). The knocked-out transcription factors were selected based on transcriptomics from a previous scale-down study, where each transcription factor seemed to be involved in the transcriptional response of *E. coli* to repeated glucose starvation (13).

Seed cultures

Seed cultures were inoculated with 100 µL of glycerol stocks into 500-mL shaking flasks with 20 mL of minimal media with the following composition (per liter): 2 g glucose, 6.8 g Na_2HPO_4, 3 g KH_2PO_4, 0.5 g NaCl, 1 g NH_4Cl, 0.49 g $MgSO_4 \times 7H_2O$, 16.95 mg $CaCl_2 \times 2H_2O$, 7.5 mg Na_2 $EDTA \times 2H_2O$, 2.25 mg $ZnSO_4 \times 7H_2O$, 0.035 mg $MnCl_2 \times 4 H_2O$, 0.15 mg $CoCl_2 \times 6H_2O$, 0.1 mg $CuSO_4 \times 2H_2O$, 0.2 mg $Na_2MoO_4 \times 2H_2O$, 1.5 mg $FeSO_4 \times 7H_2O$, 0.5 mg H_3BO_3, 0.05 mg KI, 10 µg pyridoxine HCl, 5 µg thiamine HCl, 5 µg riboflavin, 5 µg nicotinic acid, 5 µg calcium D-(+)-pantothenate, 5 µg p-aminobenzoic acid, 5 µg thioctic acid, 2 µg biotin, 2 µg folic acid, and 0.1 µg vitamin B12. Seed cultures were grown overnight at 30 °C, 225 rpm shaking speed, and 5 cm shaking diameter in a Kühner incubator (Germany).

Fed-batch fermentation

Fed-batch cultivations were carried out in the Sartorius Ambr 250 high-throughput system (Göttingen, Germany) with an initial volume of 100 mL. The minimal medium for the initial batch phase contained (per liter) 20 g glucose, 10 g $(NH_4)_2SO_4$, 15 g KH_2PO_4, 0.49 g $MgSO_4$, 0.1 g thiamine HCl, 1 mL trace metal stock solution, 1 mL iron stock solution, and 0.5 mL Antifoam 204. During the initial batch phase, DO was controlled to not fall below 40% air saturation by adjusting first the stirring speed between 1,000 and 4,000 rpm and second the aeration rate between 0.1 and 0.25 Lmin^{-1}. Upon depletion of the initial glucose amount (detected by an increase in DO), the feeding phase was initiated. DO control was switched off, and stirring speed and aeration rate were set to constant values of 4,000 rpm and 0.25 Lmin^{-1}, respectively. The feeding phase lasted 60 h starting at a feed rate of 0.4 mLh^{-1} and following an exponential ramp with the

exponential term $\mu_{set} = 0.05$ h^{-1}. In contrast to the control fed-batch cultivations, where the feed solution was supplied continuously, the feed solution was supplied discontinuously in intermittent feeding intervals in the scale-down fed-batch cultivations. One intermittent feeding interval lasted 150 s, within which the feeding pump was switched on for 60 s and switched off for 90 s (Fig. 1B). These intervals were continuously repeated throughout the feeding phase of the scale-down cultivations. The feed rate during the intermittent feeding intervals was controlled in such manner that an equal amount of feed solution was added in scale-down cultivations compared with control cultivations. The feed solution contained (per liter) 500 g glucose, 15 g KH_2PO_4, 13.7 g $MgSO_4 \times 7H_2O$, 5 mL trace metal stock solution, and 5 mL iron stock solution. Trace metal stock solution contained (per liter) 0.33 g $CuSO_4 \times 5H_2O$, 0.54 g $CoCl_2 \times 6H_2O$, 2 g $CaCl_2 \times 2H_2O$, 0.41 g $MnSO_4 \times H_2O$, 0.3 g $Na_2MoO_4 \times 2H_2O$, and 6.3 g $ZnSO_4 \times 7H_2O$. Iron stock solution contained (per liter) 30.5 g $FeCl_3 \times 6H_2O$ and 250 g citric acid $\times H_2O$. The pH was kept constant at 6.5 by titrating 8% ammonium hydroxide solution.

Bioreactor compartment model

For modeling of mixing gradients in large bioreactors, a compartment model of a 90-m³ STR with four Rushton turbines was constructed. The bioreactor geometry and operating parameters stirrer speed $N = 2.33$ s^{-1}, gas inflow $F_g = 0.79$ kgs^{-1}, and head pressure $p_{head} = 1$ bar from Nadal-Rey et al. (61) were used. The bioreactor volume was divided by three horizontal planes at half distance between the impellers, resulting in four vertically distributed compartments. Liquid exchange flows between two neighboring compartments i and j were estimated from the volumetric pumping capacity of the Rushton turbines under aeration $\emptyset_{P,g}$ with the assumption that half of an impellers volumetric discharge is directed downwards and the other half upwards. A detailed description of the compartment model design is presented in Supplementary Information. A black-box Monod kinetic model was used to simulate substrate uptake of *E. coli* in order obtain glucose gradients from the compartment model. Ordinary differential equations were solved using the *odeint* solver from the submodule *integrate* of the python library *scipy* (62).

Analytical methods

For the glucose and organic acid measurements, samples were centrifuged for 5 min at 5,000 rpm at 4 °C. The supernatant was then diluted 5-fold with the TECAN Fluent Automation System with 9 mM sulfuric acid. After filtering through a 0.22-µm filter plate, the diluted samples were measured via the UltiMate 3000 HPLC (Thermo Scientific, USA) with 9 mM sulfuric acid as the mobile phase and a flow rate of 0.7 mL/min and the Rezex ROA-Organic Acid H$^+$ (8%) column (Phenomenex, USA) as the stationary phase. The quantification of the compounds was based on the refractive index chromatograms. For cell dry weight (CDW) determination, 2 mL of culture broth was removed from the bioreactors, transferred into preweighed sample tubes, and centrifuged at 12,000 rpm for 5 min. The supernatant was removed, and the cell pellets were washed twice with 0.9% NaCl solution before drying for 24 h. The dried samples were weighed to calculate CDW. Sampling was performed in technical triplicates.

Calculations and statistical tests

The concentration measurements were used to derive the net consumed substrate, and net formed biomass, as well as the net formation of all organic acids. First, the residual mass of the

Table 1. List of *E. coli* strains tested in this study.

Strain ID	Background	Genotype	Description
WT	*E. coli* BW25113	Δ*fhuA*	Parent strain (wild type)
Δ*cra*	*E. coli* BW25113	Δ*fhuA* Δ*cra*	*cra* knockout
Δ*crp*	*E. coli* BW25113	Δ*fhuA* Δ*crp*	*crp* knockout
Δ*fliA*	*E. coli* BW25113	Δ*fhuA* Δ*fliA*	*fliA*-knockout
Δ*prpR*	*E. coli* BW25113	Δ*fhuA* Δ*prpR*	*prpR* knockout
Δ*rpoS*	*E. coli* BW25113	Δ*fhuA* Δ*rpoS*	*rpoS* knockout

Strains are referred to by their strain ID.

compound of interest i, m_i, was calculated by multiplying the measured concentration c_i with the liquid volume V_L (Eq. 1), which was exported along with the online data from the Ambr 250 system. The general formula for the net formation of a compound $m_{i,net}$ is a mass balance equation of all in- and outflows (Eq. 2), which includes the current residual mass present in the bioreactor m_i, the addition by feeding, the initial amount supplied by the batch medium $m_{i,init}$, and the lost mass of compounds by sampling $m_{i,lost}$. The total mass of lost compound at any given time point was the cumulative sum of lost compound mass at all previous sampling time points (Eq. 3).

$$m_i = c_i \times V_L \tag{1}$$

$$m_{i,net} = m_i - V_{feed} \times c_{i,feed} - m_{i,init} + m_{i,lost} \tag{2}$$

$$m_{lost,i} = \sum_{n=0}^{t-1} c_{i,n} \times V_{sample,n} \tag{3}$$

Two-factor ANOVA tests were performed to test the statistical significance of differences between values of the biomass yield Y_{SX} and the CO_2 yield Y_{SC} for the experiment design factors genotype and fermentation conditions (control, scale-down) using the python libraries *scipy* (62), *statsmodels* (63), and *bioinfokit* (64).

RNA-seq and iModulon analysis

All transcriptome samples were collected and prepared in biological triplicates. At the end of each fed-batch culture, 0.5 mL of the culture broth was added to 6 mL of Qiagen RNA-protect Bacteria Reagent. This solution was mixed by vortexing, incubated at room temperature for 5 min, and centrifuged. The supernatant was removed, and the cell pellets were stored at −70 °C. For total RNA extraction, the RNeasy Mini Kit (Qiagen) was used per vendor protocol, including on-columns DNase treatment for 30 min at room temperature. Ribosomal RNA removal, library preparation, and sequencing were performed by an external research partner (BGI Europe A/S, Denmark). RNA-seq reads were processed, as described previously (github.com/avsastry/modulome-workflow) (18). For the resulting RNA-seq datasets from this study, iModulon activities were inferred from the public *E. coli* iModulon database PRECISE-1K (github.com/SBRG/precise1k) as previously described (github.com/SBRG/precise1k-analyze) (19). DiMAs were calculated as described previously (18). Analysis and plotting of the iModulon data were performed using the python library *pymodulon* (pymodulon.readthedocs.io) (18) and with the help of iModulonDB (65). For comparison between scale-down and control culture samples, a difference in iModulon activity of ±2 and a false detection rate (FDR) of <0.1 was applied.

DGE and statistical enrichment

DGE analysis was performed with DESeq2 in R (66). For the comparison of gene expression between scale-down and control cultures of the six tested *E. coli* strains, a fold change of ±1.5 with an adjusted P-value of <0.05 was considered significantly up-/down-regulated. Gene annotation of COGs and regulons was obtained from iModulonDB (65) and from RegulonDB (67). Computation of statistically significant enrichments of COGs and regulons among the up- and down-regulated genes was performed using built-in function of *pymodulon*.

Acknowledgments

The authors thank Christina Lenhard for support on strain construction. The authors thank Amy Lou, Joshua Burrows, and Griffith Hughes from the Systems Biology Research Group, University of California, for providing feedback on the iModulon analysis.

Supplementary Material

Supplementary material is available at *PNAS Nexus* online.

Funding

Author Contributions

J.B-R.: lead methodology, software, lead formal analysis, lead investigation, lead data curation, lead writing—original draft preparation, and visualization; Y.D.B.: supporting investigation and supporting data curation; J.V.O.: supporting methodology, supporting investigation, and supporting writing—original draft preparation; S.Ø.: supporting formal analysis and supporting data curation; L.Y.: resources; D.Z.: supporting conceptualization, supporting writing—review and editing, and supporting supervision; and S.S.: lead conceptualization, lead writing—review and editing, lead supervision, and project administration.

Data Availability

This work uses the ICA of *E. coli* transcriptomes dataset PRECISE-1K from iModulonDB (65). Additionally, the RNA-seq dataset reported in Löffler et al (13) was used. Data of the raw sequence reads from RNA-seq samples generated in this work are available at: ncbi.nlm.nih.gov/bioproject/1061466. All computer code and data files are available at: github.com/jonruh/Effects-of-glucose-oscillations-on-E.-coli.git.

References

1. Noorman HJ, Heijnen JJ. 2017. Biochemical engineering's grand adventure. *Chem Eng Sci*. 170:677–693.
2. Straathof AJJ, *et al.* 2019. Grand research challenges for sustainable industrial biotechnology. *Trends Biotechnol*. 37(10):1042–1050.
3. Nadal-Rey G, *et al.* 2021. Understanding gradients in industrial bioreactors. *Biotechnol Adv*. 46:107660.
4. Larsson G, *et al.* 1996. Substrate gradients in bioreactors: origin and consequences. *Bioprocess Eng*. 14(6):281–289.
5. Noorman H. 2011. An industrial perspective on bioreactor scale-down: what we can learn from combined large-scale bioprocess and model fluid studies. *Biotechnol J*. 6(8):934–943.
6. Neubauer P, Junne S. 2010. Scale-down simulators for metabolic analysis of large-scale bioprocesses. *Curr Opin Biotechnol*. 21(1):114–121.
7. Sweere APJ, Luyben KCAM, Kossen NWF. 1987. Regime analysis and scale-down: tools to investigate the performance of bioreactors. *Enzyme Microb Technol*. 9(7):386–398.
8. George S, Larsson G, Enfors SO. 1993. A scale-down two-compartment reactor with controlled substrate oscillations: metabolic response of *Saccharomyces cerevisiae*. *Bioprocess Eng*. 9(6):249–257.
9. Wang G, *et al.* 2018. Comparative performance of different scale-down simulators of substrate gradients in *Penicillium chrysogenum*

cultures: the need of a biological systems response analysis. *Microb Biotechnol*. 11(3):486–497.

10 Haringa C, *et al*. 2016. Euler-Lagrange computational fluid dynamics for (bio)reactor scale down: an analysis of organism lifelines. *Eng Life Sci*. 16(7):652–663.

11 Haringa C, Deshmukh AT, Mudde RF, Noorman HJ. 2017. Euler-Lagrange analysis towards representative down-scaling of a 22 m³ aerobic S. cerevisiae fermentation. *Chem Eng Sci*. 170: 653–669.

12 Haringa C, Mudde RF, Noorman HJ. 2018. From industrial fermentor to CFD-guided downscaling: what have we learned? *Biochem Eng J*. 140:57–71.

13 Löffler M, *et al*. 2016. Engineering *E. coli* for large-scale production—strategies considering ATP expenses and transcriptional responses. *Metab Eng*. 38:73–85.

14 Löffler M, *et al*. 2017. Switching between nitrogen and glucose limitation: unraveling transcriptional dynamics in *Escherichia coli*. *J Biotechnol*. 258:2–12.

15 von Wulffen J, Ulmer A, Jäger G, Sawodny O, Feuer R. 2017. Rapid sampling of *Escherichia coli* after changing oxygen conditions reveals transcriptional dynamics. *Genes (Basel)*. 8(3):90.

16 Myers KS, Park DM, Beauchene NA, Kiley PJ. 2015. Defining bacterial regulons using ChIP-seq. *Methods*. 86:80–88.

17 Browning DF, Busby SJW. 2016. Local and global regulation of transcription initiation in bacteria. *Nat Rev Microbiol*. 14(10): 638–650.

18 Sastry AV, *et al*. 2019. The *Escherichia coli* transcriptome mostly consists of independently regulated modules. *Nat Commun*. 10(1):5536.

19 Lamoureux CR, *et al*. 2023. A multi-scale expression and regulation knowledge base for *Escherichia coli*. *Nucleic Acids Res*. 51(19): 10176–10193.

20 Rychel K, *et al*. 2023. Laboratory evolution, transcriptomics, and modeling reveal mechanisms of paraquat tolerance. *Cell Rep*. 42(9):113105.

21 Tang W, *et al*. 2017. A 9-pool metabolic structured kinetic model describing days to seconds dynamics of growth and product formation by *Penicillium chrysogenum*. *Biotechnol Bioeng*. 114(8): 1733–1743.

22 Heijnen JJ, Kleerebezem R. 2010. Bioenergetics of microbial growth. *Encycl Ind Biotechnol*. 1–66. doi:10.1002/9780470054581.eib084

23 Battesti A, Majdalani N, Gottesman S. 2011. The RpoS-mediated general stress response in *Escherichia coli*. *Annu Rev Microbiol*. 65: 189–213.

24 Hardiman T, Lemuth K, Keller MA, Reuss M, Siemann-Herzberg M. 2007. Topology of the global regulatory network of carbon limitation in *Escherichia coli*. *J Biotechnol*. 132(4):359–374.

25 Wendrich TM, Blaha G, Wilson DN, Marahiel MA, Nierhaus KH. 2002. Dissection of the mechanism for the stringent factor RelA. *Mol Cell*. 10(4):779–788.

26 Irving SE, Choudhury NR, Corrigan RM. 2021. The stringent response and physiological roles of (pp)pGpp in bacteria. *Nat Rev Microbiol*. 19(4):256–271.

27 Boutte CC, Crosson S. 2013. Bacterial lifestyle shapes stringent response activation. *Trends Microbiol*. 21(4):174–180.

28 Ziegler M, Zieringer J, Takors R. 2020. Transcriptional profiling of the stringent response mutant strain *E. coli* SR reveals enhanced robustness to large-scale conditions. *Microb Biotechnol*. 14: 993–1010.

29 Franchini AG, Ihssen J, Egli T. 2015. Effect of global regulators RpoS and cyclic-AMP/CRP on the catabolome and transcriptome of *Escherichia coli* K12 during carbon- and energy-limited growth. *PLoS One*. 10(7):e0133793.

30 Imlay JA. 2013. The molecular mechanisms and physiological consequences of oxidative stress: lessons from a model bacterium. *Nat Rev Microbiol*. 11(7):443–454.

31 Yang L, *et al*. 2019. Cellular responses to reactive oxygen species are predicted from molecular mechanisms. *Proc Natl Acad Sci U S A*. 116(28):14368–14373.

32 Fasnacht M, Polacek N. 2021. Oxidative stress in bacteria and the central dogma of molecular biology. *Front Mol Biosci*. 8:671037.

33 Seo SW, *et al*. 2014. Deciphering fur transcriptional regulatory network highlights its complex role beyond iron metabolism in *Escherichia coli*. *Nat Commun*. 5:4910.

34 Dwyer DJ, Kohanski MA, Collins JJ. 2009. Role of reactive oxygen species in antibiotic action and resistance. *Curr Opin Microbiol*. 12(5):482–489.

35 Fontenot CR, Ding H. 2023. Ferric uptake regulator (Fur) binds a [2Fe-2S] cluster to regulate intracellular iron homeostasis in *Escherichia coli*. *J Biol Chem*. 299(6):104748.

36 Navasa N, *et al*. 2019. The role of RcsA in the adaptation and survival of *Escherichia coli* K92. *FEMS Microbiol Lett*. 366(8):fnz082.

37 Wang C, *et al*. 2020. Colanic acid biosynthesis in *Escherichia coli* is dependent on lipopolysaccharide structure and glucose availability. *Microbiol Res*. 239:126527.

38 Meng J, Young G, Chen J. 2021. The Rcs system in Enterobacteriaceae: envelope stress responses and virulence regulation. *Front Microbiol*. 12:627104.

39 Schneider BL, Hernandez VJ, Reitzer L. 2013. Putrescine catabolism is a metabolic response to several stresses in *Escherichia coli*. *Mol Microbiol*. 88(3):537–550.

40 Ramseier TM. 1996. Cra and the control of carbon flux via metabolic pathways. *Res Microbiol*. 147(6–7):489–493.

41 Sarkar D, Siddiquee KAZ, Araúzo-Bravo MJ, Oba T, Shimizu K. 2008. Effect of cra gene knockout together with edd and iclR genes knockout on the metabolism in *Escherichia coli*. *Arch Microbiol*. 190(5):559–571.

42 Saier MH, Ramseier TM. 1996. The catabolite repressor/activator (Cra) protein of enteric bacteria. *J Bacteriol*. 178(12):3411–3417.

43 Perrenoud A, Sauer U. 2005. Impact of global transcriptional regulation by ArcA, ArcB, Cra, Crp, Cya, Fnr, and Mlc on glucose catabolism in *Escherichia coli*. *J Bacteriol*. 187(9):3171–3179.

44 Fitzgerald DM, Bonocora RP, Wade JT. 2014. Comprehensive mapping of the *Escherichia coli* flagellar regulatory network. *PLoS Genet*. 10(10):e1004649.

45 Enfors SO, *et al*. 2001. Physiological responses to mixing in large scale bioreactors. *J Biotechnol*. 85(2):175–185.

46 Lapin A, Schmid J, Reuss M. 2006. Modeling the dynamics of *E. coli* populations in the three-dimensional turbulent field of a stirred-tank bioreactor-A structured-segregated approach. *Chem Eng Sci*. 61(14):4783–4797.

47 Brock M, Maerker C, Schütz A, Völker U, Buckel W. 2002. Oxidation of propionate to pyruvate in *Escherichia coli*: involvement of methylcitrate dehydratase and aconitase. *Eur J Biochem*. 269(24):6184–6194.

48 Basan M, *et al*. 2015. Overflow metabolism in *Escherichia coli* results from efficient proteome allocation. *Nature*. 528(7580): 99–104.

49 Pal A, Iyer MS, Srinivasan S, Narain Seshasayee AS, Venkatesh KV. 2022. Erratum: global pleiotropic effects in adaptively evolved *Escherichia coli* lacking CRP reveal molecular mechanisms that define the growth physiology. *Open Biol*. 12(4):220087.

50 Valgepea K, *et al*. 2010. Systems biology approach reveals that overflow metabolism of acetate in *Escherichia coli* is triggered by

carbon catabolite repression of acetyl-CoA synthetase. *BMC Syst Biol*. 4(1):166.

51 Cheng C, *et al.* 2019. Laboratory evolution reveals a two-dimensional rate-yield tradeoff in microbial metabolism. *PLoS Comput Biol*. 15(6):e1007066.

52 Son YJ, Phue JN, Trinh LB, Lee SJ, Shiloach J. 2011. The role of Cra in regulating acetate excretion and osmotic tolerance in *E. coli* K-12 and *E. coli* B at high density growth. *Microb Cell Fact*. 10:52.

53 Ziegler M, *et al.* 2021. Engineering of a robust *Escherichia coli* chassis and exploitation for large-scale production processes. *Metab Eng*. 67:75–87.

54 Dong T, Yu R, Schellhorn H. 2011. Antagonistic regulation of motility and transcriptome expression by RpoN and RpoS in *Escherichia coli*. *Mol Microbiol*. 79(2):375–386.

55 Brand E, Junne S, Anane E, Cruz-Bournazou MN, Neubauer P. 2018. Importance of the cultivation history for the response of *Escherichia coli* to oscillations in scale-down experiments. *Bioprocess Biosyst Eng*. 41(9):1305–1313.

56 Vasilakou E, van Loosdrecht MCM, Wahl AS. 2020. *Escherichia coli* metabolism under short-term repetitive substrate dynamics: adaptation and trade-offs. *Microb Cell Fact*. 19:116.

57 Gecse G. 2022. *Characterisation and optimisation of Escherichia coli cell factories for large-scale industrial production of human milk oligosaccharides*. Technical University of Denmark.

58 Law RC, Nurwono G, Park JO. 2024. A parallel glycolysis provides a selective advantage through rapid growth acceleration. *Nat Chem Biol*. 20(3):314–322.

59 Baba T, *et al.* 2006. Construction of *Escherichia coli* K-12 in-frame, single-gene knockout mutants: the Keio collection. *Mol Syst Biol*. 2:2006.0008.

60 Jensen SI, Lennen RM, Herrgård MJ, Nielsen AT. 2015. Seven gene deletions in seven days: fast generation of *Escherichia coli* strains tolerant to acetate and osmotic stress. *Sci Rep*. 5:17874.

61 Nadal-Rey G, *et al.* 2021. Development of dynamic compartment models for industrial aerobic fed-batch fermentation processes. *Chem Eng J*. 420:130402.

62 Virtanen P, *et al.* 2020. Scipy 1.0: fundamental algorithms for scientific computing in python. *Nat Methods*. 17(3):261–272.

63 Seabold S, Perktold J. 2010. Statsmodels: econometric and statistical modeling with python. Proceedings of the 9th Python in Science Conference, Austin, Texas. SciPy; 2010. p. 92–96. https://doi.org/10.25080/Majora-92bf1922-011

64 Bedre R. 2022. reneshbedre/bioinfokit: bioinformatics data analysis and visualization toolkit (2.0.9). *Zenodo*. https://doi.org/10.5281/zenodo.3964972 Date of deposit 10 April 2020.

65 Rychel K, *et al.* 2021. IModulonDB: a knowledgebase of microbial transcriptional regulation derived from machine learning. *Nucleic Acids Res*. 49(D1):D112–D120.

66 Love MI, Huber W, Anders S. 2014. Moderated estimation of fold change and dispersion for RNA-seq data with DESeq2. *Genome Biol*. 15(12):550.

67 Tierrafría VH, *et al.* 2022. RegulonDB 11.0: comprehensive high-throughput datasets on transcriptional regulation in *Escherichia coli* K-12. *Microb Genom*. 8(5):mgen000833.